Heat transfer study and optimization of nanofluid triangular cavity with a pentagonal barrier by finite element approach and RSM

Kh. Hosseinzadeh [a,b,*], M. Roshani [b], M.A. Attar [b], D.D. Ganji [b], Mohammad Behshad Shafii [a,c]

[a] *Department of Mechanical Engineering, Sharif University of Technology, Azadi Ave, Tehran, Iran*
[b] *Department of Mechanical Engineering, Babol Noshirvani University of Technology, Babol, Iran*
[c] *Sharif Energy, Water and Environment Institute (SEWEI), Tehran, Iran*

ARTICLE INFO

Keywords:
Triangular cavity
Mixed convection
Magnetohydrodynamics
Nanofluid
Optimization

ABSTRACT

Nowadays, several engineering applications and academic investigations have demonstrated the significance of heat transfers in general and mixed convection heat transfer (MCHT) in particular in cavities containing obstacles. This study's main goal is to analyze the MCHT of a nanofluid in a triangular cavity with a pentagonal barrier using magneto hydrodynamics (MHD). The cavity's-oriented walls are continuous cold temperature, whereas the bottom wall of the triangle and all pentagonal obstacle walls are kept at a constant high temperature. For solving governing equations, we utilized the Galerkin's finite element approach. Four dimensionless factors, Richardson number ($0.01 \leq \mathrm{Ri} \leq 5$), Reynolds number ($10 \leq \mathrm{Re} \leq 50$), Buoyancy ratio ($0.01 \leq \mathrm{Br} \leq 10$) and Hartmann number ($0 \leq Ha \leq 20$) are examined for their effects on streamlines, isotherms, concentration, velocity, and the Nusselt number. Also, with the help of Taguchi method and Response Surface Method (RSM) the optimization of the studied dimensionless parameters has been done. The optimum values of Ri, Re, Ha and Br are obtained 4.95, 30.49, 18.35 and 0.05 respectively. Ultimately, a correlation has been extracted for obtaining the optimum average Nusselt number (Nu) in mentioned cavity.

1. Introduction

Numerous biological and economic phenomena depend critically and unquestionably on heat transfer. One of the heat transfer techniques that combines forced and natural convection is mixed convection. Due to its potential use in engineering fields many studies have been done. For instance, in heat exchangers which studied by Chen et al. [1] presents that increasing the tube diameter in a vertical annular finned tube heat exchanger resulted in a higher Nusselt number, while decreasing the diameter led to a higher friction factor. In electronic board cooling, the work of Mathew et al. [2] expresses the optimal arrangement of IC chips mounted on an SMPS board for efficient cooling under mixed convection was a staggered arrangement with a pitch of 20 mm. For ventilation in buildings Wurtz et al. [3] study indicates that modular zonal models are effective tools for simulating natural and mixed convection in buildings with 2D and 3D configurations. In solar collectors Xiao et al. [4] research shows that the performance of a solar collector can be

---

enhanced by utilizing microalgae slurry as a heat transfer fluid, with laminar mixed convection playing a crucial role in the heat transfer process. A study of a microchannel by Tavakoli et al. [5] demonstrates that the two-phase approach was more effective than the single-phase approach in predicting mixed convection heat transfer inside a vertical microchannel. Moreover, in the field of automotive a study by Hussein et al. [6] illustrates that the addition of Al2O3 nanoparticles to the base fluid significantly improved the heat transfer performance of the automotive cooling system under forced convection and many other industrial applications, there has been a lot of interests in the field of MCHT. Plus, the major objective for all mentioned fields is to fend the extra heat and improve cooling the systems.

Recently, the study of heat transfers in various cavities which are common in industrial applications has become popular. These cavities may contain obstacles, or some of their walls may be lid driven, or they may have different geometries, such as circular, trapezoidal, triangular, square etc. [7–10]. To better understand the MCHT, extensive efforts have been carried out. Steady state heat convection in an enclosure for combination of mass and temperature gradients was originally researched by Al-Amiri et al. [11]. The transport phenomena were studied using a number of crucial operational dimensionless parameters. The factors under consideration were the Ri number, Lewis number (Le) and parameter of Br. Into the enclosure when Ri value was low, the properties of heat transfer and mass transfer are improved as evident predominant effect of the mechanical action caused by the sliding lid. Apurba Kumar Santra et al. [12] quantitatively investigated the improvement of heat transport in a square enclosure using copper-water Nanofluid for variety of Rayleigh number (Ra) and volume fraction of solids. For most any Ra, the outcomes demonstrate increasing the solid volume fraction reduces heat transport significantly. When Ra exceeds 3%, however, the heat transmission is virtually constant at low Rayleigh numbers. Ghasemi and Aminossadati [13] numerically studied convection in a triangular enclosure which had driven lids and also it was filled with water and Al_2O_3 solid particles. Their results showed that by increasing the volume fraction of Al_2O_3 in water, the heat transfer rate increases for all Ri values. Sivasankaran et al. [14] Investigated MCHT in a cavity which was lid-driven and affected by inconsistent heating. They understood that if both walls were heated non-uniform, the rate of heat transfer would increase. In a triangle shaped cavity Hasanuzzaman et al. [15] analyzed the MCHT and investigated the effect of Le changes on temperature and concentration behavior. They claimed that heat transfer diminishes as the Lewis number increases. Whereas, the rate of mass transfer increases by 32% with raising Le from 5 to 20. Litan Kumar Saha et al. [16] have numerically analyzed a MCHT flow issue which involved an electrically charged fluid in a hollow under an externally imposed homogeneous electromagnetic force, which includes the influence of internal heat production. For forced convection dominated regions. The importance of generation or absorption of heat becomes negligible. However, it has a serious impact for larger values of Richardson number and the field of magnetism has played a major job in controlling Flow of fluids and heat pass. The MCHT of nanofluid was modeled in a 3-D cubical hollow with numerous pairs of cooling and heating within by Garoosi et al. [17] They concluded that as the nanoparticle diameter decreased and Richardson's number increased, the rate of heat transfer increased. Haq et al. [18] Explored the phenomenon of natural convection in an enclosure which had the shape of trapezius and was heated and containing Single Wall Carbon Nanotubes. They observed that the flow streamlines and thermal contours wemagnre both strengthened via increasing the Rayleigh number. In a rhombus cavity with a square in the center, the effect of the presence of copper monoxide nanoparticles in water on heat transfer also has been probed by Haq et al. [19] They investigated the thermal and flow fields which were affected when the inner barrier was cooled or adiabatic or heated. Al-Kouz et al. [20] studied natural convection in a sloped square cavity with two fins attached to the hot wall. Finally, a correlation was suggested for Nu number associated with studied parameters. Munshi et al. [21] examined the effects of a large variety of non-dimensional numbers on the convection heat transfer mechanism in a lid-driven hexagonal enclosure with corner heater, including Ri and Ha numbers. They had claimed that increasing the Ha number causes a significant reduction in convective current in the enclosure, and the properties of the flow and mechanisms of heat transfer inside the hexagonal cavity are firmly influenced by the Ri number. As a result, a high Ri number increases the lid-driven impact, whereas a low Ri number increases the influence of the heat source on the flow and heat properties. Selimefendigil [22] has analyzed a lid-driven cavity with an internal elliptic obstacle and nanotubes with single and multiple walls and also, reported that the heat transfer rate improved by 120.20% in solid volume fraction 0.06 relative to purified water. Haq and S. Aman [23] explored the CuO-water nanofluid flow within a cavity shaped like trapezium with an interior heated obstruction, and the issue was numerically addressed utilizing the Finite Element Method (FEM). These simulations are run for various lengths of heated region, Ra number, nanoparticles volume fraction, Aspect ratio, and several kinds of interior square cylinders in this model. Inside a rhombic enclosure with nanoparticle Cu mixed with water within, Dutta et al. [24] explored the magneto-fluid dynamics (MHD) natural convection and mechanisms of entropy generation. They numerically simulated for various Ra numbers ($10^3 \leq$ Ra $\leq 10^6$), Ha number ($0 \leq Ha \leq 100$) and three different slope angles of 30, 45 and 60° and also considered different volume fractions. They observed that by increasing the slope angle the Nu_{avg} number increases in diffusion dominated zone and also the total entropy generation rate declines with the increase of Ha for all values of Ra and slope angles of the enclosure. In a square cavity filled with SWCNTs, Haq et al. [25] computationally investigated the impact of different locations of bottom warmed parallel fins. They described how quickly heat transferred when nanoparticles were available. Inside a trapezoidal enclosure filled with elliptic shaped obstacle Saqib Shah et al. [26] perused the impact of changing some dimensionless numbers including Le, Ri, Re numbers and buoyancy ratio parameter. They also studied the effect of moving partial lid walls at top of trapezoidal cavity. They deduced that rate of mass transfer highly increases by increasing the Lewis number. They also observed that isotherms are more impacted by moving partial lid walls. M. Bahiraei et al. [27] simulated the flow of Ag-water nanofluid inside an elliptical pin-fin heat sink. Entropy generation and exergy considerations were analyzed. Results showed that increasing nanoparticle concentration and decreasing aspect ratio reduced entropy generation. M. Bahiraei [28] presents a study on the heat transfer characteristics of nanofluids using a numerical simulation method. This study contributes to the understanding of the heat transfer behavior of nanofluids, which has important implications for engineering applications. M. Amani, P. Amani, M. Bahiraei et al. [29] provided a comprehensive overview of recent research on nanofluid flow and heat transfer between parallel surfaces. The study has discussed the
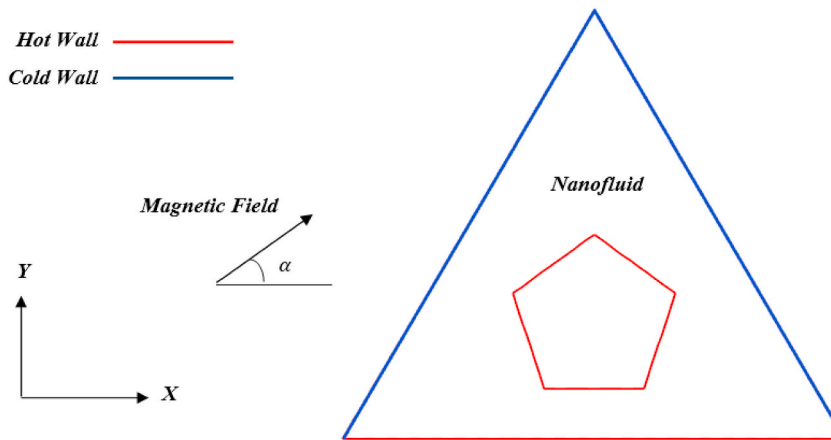
Fig. 1. Geometry of the triangular cavity and it's boundary conditions.

different types of nanofluids used, the various methods of preparation, and the different experimental techniques used to study them. N. Mazaheri and M. Bahiraei [30] presented a study on the performance of a spiral heat exchanger using different types of nanofluids. The study has focused on the energy and exergy efficiencies of the heat exchanger as well as the hydrodynamic behavior of the nanofluids. The results have indicated that the use of certain nanofluids with specific particle shapes can enhance the performance of the spiral heat exchanger, which has important implications for process intensification.

The purpose of this study is to investigate mixed convection heat transfer in a novel geometry which is a triangular cavity with a pentagonal obstacle using the FEM method. The study examines the effect of different parameters such as Reynolds number, Richardson number, Hartmann number and buoyancy ratio on the isotherms, streamlines, concentration, average *Nu*, and local *Nu*, is analyzed and demonstrated. Following that, the optimal values for Ri, Re, *Ha*, Br, and average *Nu* were calculated by employing Taguchi's method and RSM.

The study shows that Alterations in the buoyancy ratio produce an inverse correlation with the Nusselt number, while an increase in the Br parameter leads to a substantial increase in the temperature profile surrounding the pentagonal obstacle in the cavity.

2. Problem model and formulation

Fig. 1 depicts a triangular cavity with an interior pentagonal barrier, based on the triangle's height, 0.8 L, and its length, L. Both sloped adiabatic enclosure walls are cold and the bottom one is heated as well as pentagonal barrier. Since that natural convection is a part of the heat transfer, the following relation is the Boussinesq Approximation for the fluid's density [26] (See in Eq. (1)):

$$\rho = \rho_0[1 - \beta_T(\mathrm{T} - \mathrm{T}_c) + \beta_c(\mathrm{c} - \mathrm{c}_c)], \tag{1}$$

In the preceding equation ρ_0 is the density of the fluid at $\mathrm{T}_0 = (\mathrm{T}_h + \mathrm{T}_c)/2$ and concentration is $\mathrm{c}_0 = (\mathrm{c}_h + \mathrm{c}_c)/2$.

The flow field in this problem is two-dimensional, steady, laminar, and incompressible. The governing equations for fluid flow taking into consideration the above conditions are as follows [26]:

$$\nabla.\mathrm{V} = 0, \tag{2}$$

$$\mathrm{u}\frac{\partial u}{\partial x} + v\frac{\partial u}{\partial y} = -\frac{1}{\rho}\frac{\partial p}{\partial x} + \nu\nabla^2 u, \tag{3}$$

$$\mathrm{u}\frac{\partial v}{\partial x} + v\frac{\partial v}{\partial y} = -\frac{1}{\rho}\frac{\partial p}{\partial y} + \nu\nabla^2 \mathrm{v} + g[\beta_T(\mathrm{T} - \mathrm{T}_c) + \beta_c(\mathrm{c} - \mathrm{c}_c)] - \frac{\sigma B_0^2 v}{\rho}, \tag{4}$$

$$\mathrm{u}\frac{\partial T}{\partial x} + v\frac{\partial T}{\partial y} = \alpha\nabla^2 \mathrm{T}, \tag{5}$$

$$\mathrm{u}\frac{\partial c}{\partial x} + v\frac{\partial c}{\partial y} = D\nabla^2 \mathrm{c} \tag{6}$$

in the equations above $V = (\mathrm{u}, \mathrm{v})$ and $\nabla = \left(\frac{\partial}{\partial x}, \frac{\partial}{\partial y}\right)$. The following dimensionless expressions have been substituted for the major variables in the preceding equations: (See in Eq. (7))
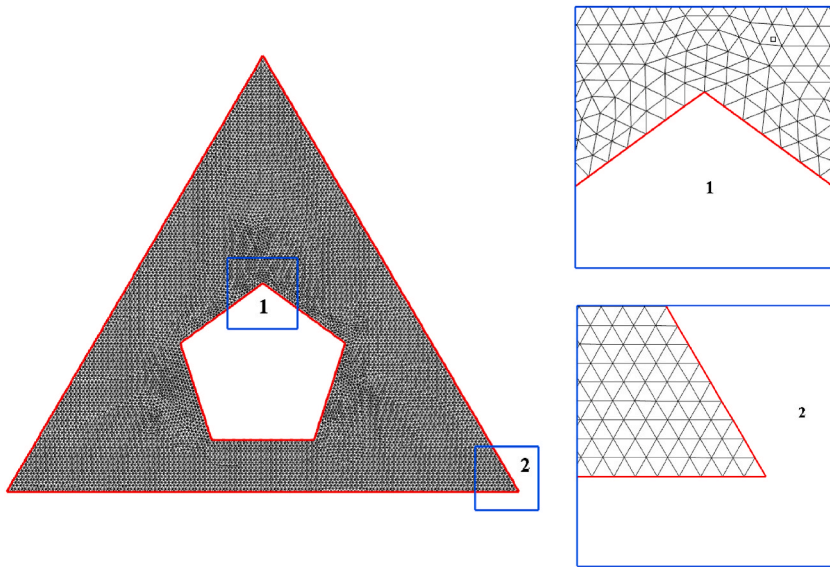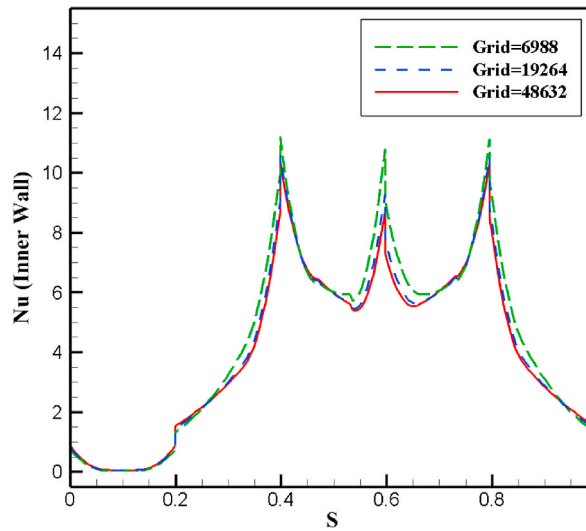
Fig. 2. Unstructured adaptive mesh.

Fig. 3. Values of local *Nu* number for different grid sizes when $\mathrm{Re} = 20, Ha = 10, Br = 5, Ri = 3, \mathrm{Pr} = 6.2$ and $Le = 1$..

$$(\mathrm{XY}) = \left(\frac{x}{L} \; \frac{y}{L}\right), (\mathrm{UV}) = \left(\frac{u}{u_0} \; \frac{v}{u_0}\right), \mathrm{T} = \mathrm{T}_c + (\mathrm{T}_h - \mathrm{T}_c)\theta, P = \frac{p}{\rho u_0}, c = c_c + (c_h - c_c)\mathrm{C}. \tag{7}$$

As a result, Equations (2)–(6) are dimensionless as bellow:

$$\frac{\partial \mathrm{U}}{\partial \mathrm{X}} + \frac{\partial \mathrm{V}}{\partial \mathrm{Y}} = 0, \tag{8}$$

$$\mathrm{U}\frac{\partial \mathrm{U}}{\partial X} + \mathrm{V}\frac{\partial \mathrm{U}}{\partial Y} = -\frac{\partial P}{\partial X} + \frac{1}{\mathrm{Re}}\nabla^2 \mathrm{U}, \tag{9}$$

$$\mathrm{U}\frac{\partial \mathrm{V}}{\partial X} + \mathrm{V}\frac{\partial \mathrm{V}}{\partial Y} = -\frac{\partial P}{\partial Y} + \frac{1}{\mathrm{Re}}\nabla^2 \mathrm{V} + \mathrm{Ri}(\theta + \mathrm{BrC}) - \mathrm{Pr}(\mathrm{Ha}^2)\mathrm{V}, \tag{10}$$

$$\mathrm{U}\frac{\partial T}{\partial X} + \mathrm{V}\frac{\partial T}{\partial Y} = \left(\frac{1}{\mathrm{RePr}}\right)\nabla^2 \theta, \tag{11}$$
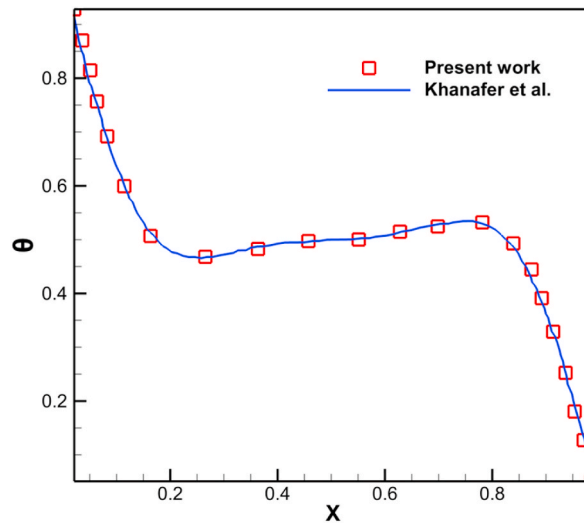
Fig. 4. Validation of the present study with Khanafer et al. [31] $\varphi = 0.05$ and Pr $= 6.2$ (Cu-Water).
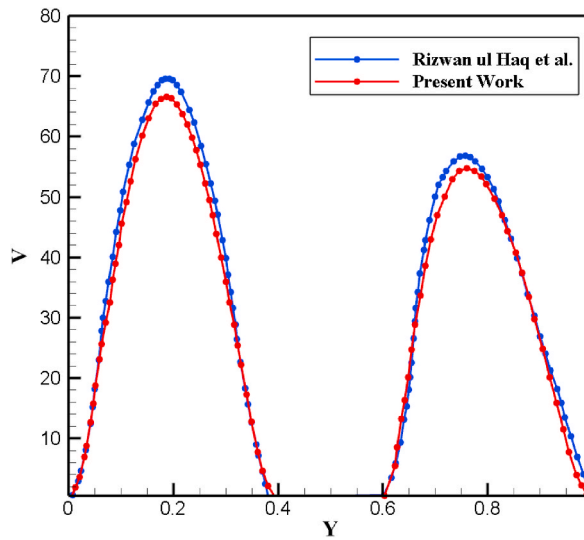

Fig. 5. The V-velocity of water base Cu nanofluid along the Y-direction at ($\varphi = 0$, Ra $= 10^5$ and LT $= 0.4$), obtained by current simulation and the results of Haq et al. [23].

$$U\frac{\partial C}{\partial X} + V\frac{\partial C}{\partial Y} = \left(\frac{1}{\text{RePrLe}}\right)\nabla^2 C. \tag{12}$$

As an outcome, the Re, Pr, Ri, *Le*, and the Br of the issue are outlined below:

$$\text{Re} = \frac{u_0 L}{\nu}, Ri = \frac{g\beta_T(T_h - T_c)L^3}{\nu^2 \text{Re}^2}, Le = \frac{\alpha}{D}, \text{Pr} = \frac{\nu}{\alpha}, Br = \frac{\beta_c(c_h - c_c)}{\beta_T(T_h - T_c)}, \text{Ha} = B_0 L\sqrt{\frac{\sigma}{\mu}}. \tag{13}$$

Now the boundary conditions' dimensionless form related to Equations 8–12 are as follows:
at the triangular cavity's bottom wall (See in Eq. 14–17):

$$(U, V) = (0, 0), \theta = 1, C = 0. \tag{14}$$

at the inclined walls of the triangular enclosure:

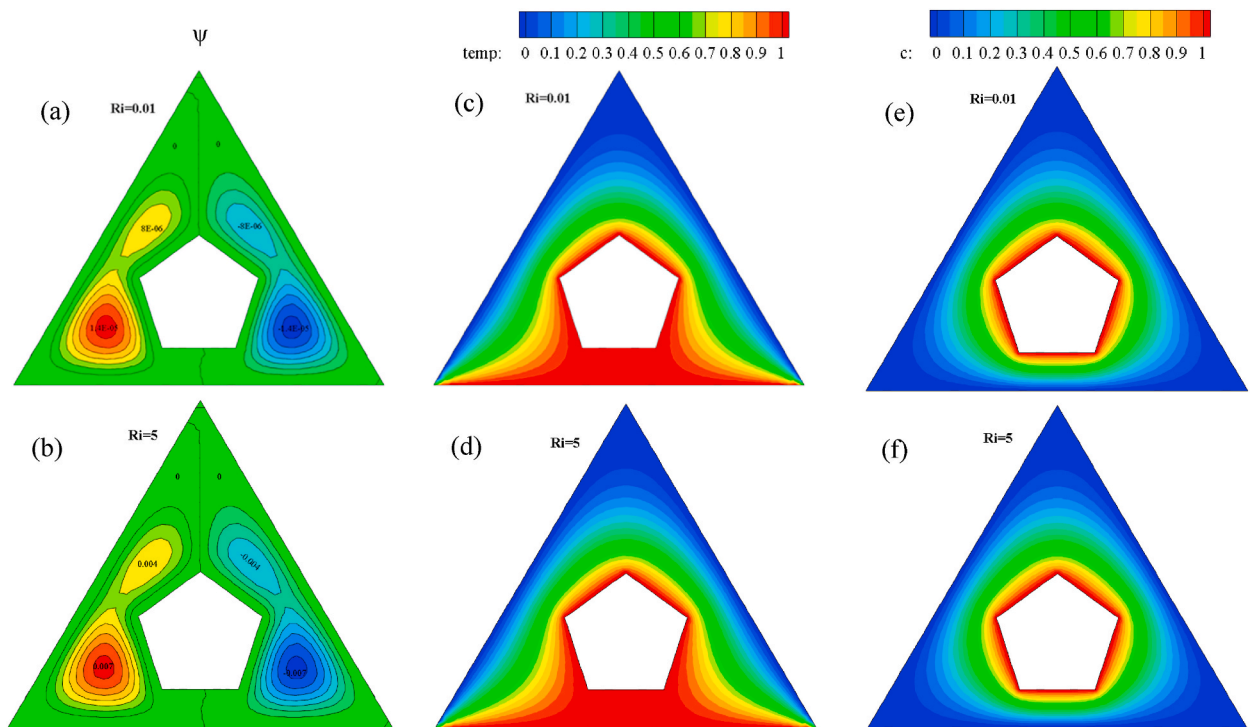$$(U, V) = (0, 0), \theta = 0, C = 0. \tag{15}$$

On the pentagonal barrier:

Fig. 6. Variation of (a–b) streamlines, (c–d) isotherms and, (e–f) concentration based on different Ri numbers.
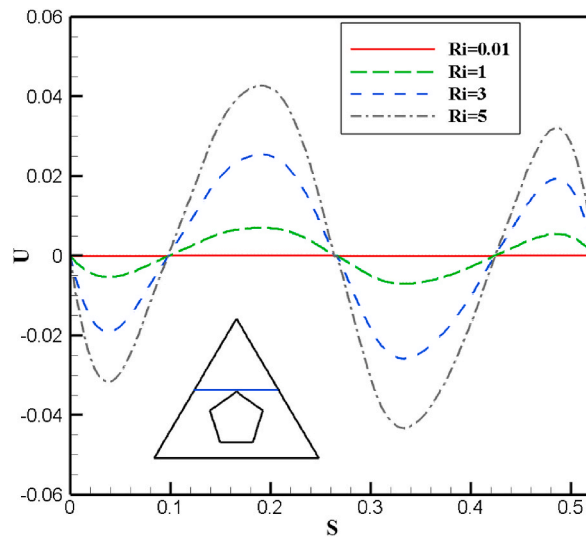

Fig. 7. Variation of U-velocity respect to different Ri.

$$(U, V) = (0, 0), \theta = C = 1, \tag{16}$$

the local *Nu* is defined as follows:

$$Nu = - \left(\frac{\partial \theta}{\partial Y} \right)_{Y=0} \tag{17}$$

The boundary conditions (14–16) are used to solve equations 8–12 using the FEM. Penalty functions were utilized to remove the pressure factor from the above equations. Hence, a penalty parameter γ in momentum equations, associates the pressure term with the continuity term in order to make the following equations easier to solve. As a result, we have the following (See in Eq. (18)):
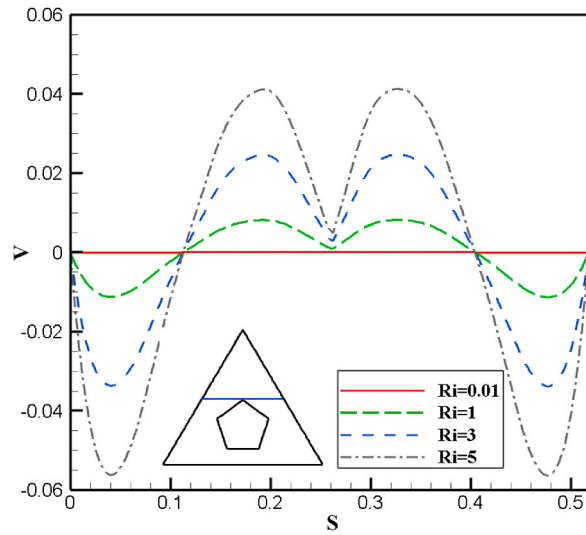
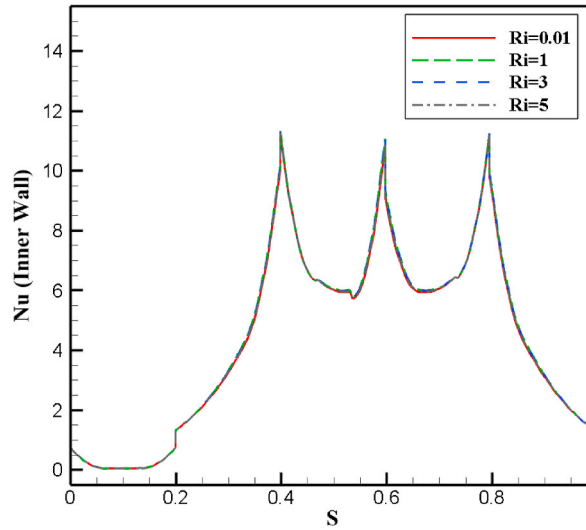**Fig. 8.** Variation of V-velocity respect to different Ri.

Fig. 9. Variation of *Nu* number respect to different Ri.

$$P = -\gamma\left(\frac{\partial U}{\partial X} + \frac{\partial V}{\partial Y}\right) \tag{18}$$

It's important to notice that the penalty parameter's value has a significant influence on the final result, which in this study has been determined 10^7. The correlations between velocity and stream functions are as below [26] (See in Eq. (19)):

$$U = \frac{\partial \psi}{\partial y}, V = -\frac{\partial \psi}{\partial X}. \tag{19}$$

3. Numerical approach, grid independency and validation assessment

For numerical simulation of this problem Flex PDE software has been used. Flex PDE is an open-source software which solves problems based on Galerkin's FEM. The Galerkin's finite element method (FEM) is a numerical technique used to solve partial differential equations (PDEs) and other mathematical problems. The FEM breaks down a complex problem into a set of smaller, simpler sub-problems that can be solved using numerical methods. It involves discretizing the problem domain into a set of finite elements, each of which is defined by a set of nodes and a set of basis functions. The basis functions are used to approximate the unknown solution within each element, and the Galerkin's method involves multiplying the PDE by a test function and integrating over each
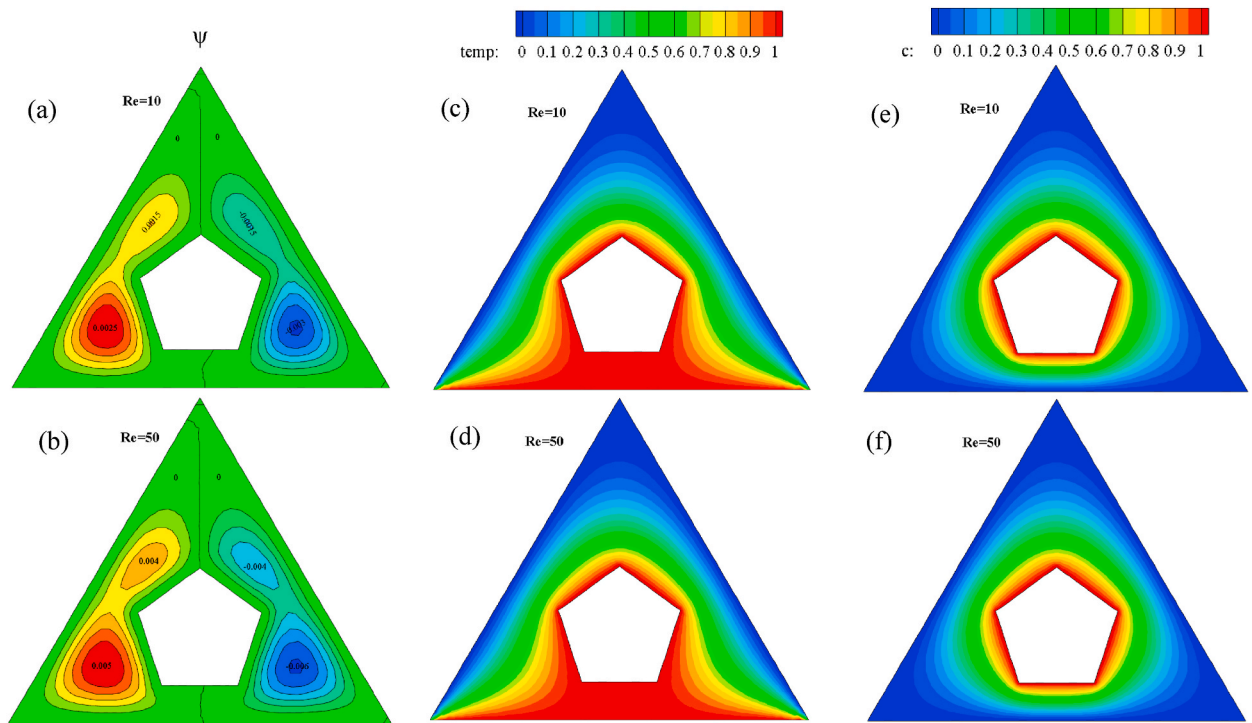
Fig. 10. Variation of (a–b) streamlines, (c–d) isotherms and, (e–f) concentration based on different Re numbers.
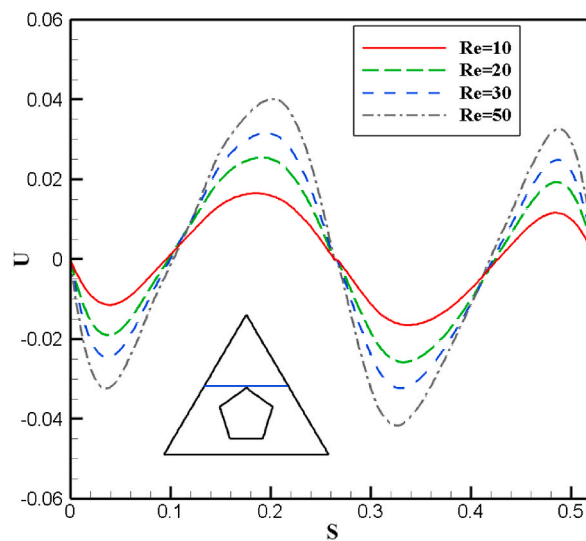

Fig. 11. Variation of U-velocity respect to different Re

element. Overall, the Galerkin's FEM is a powerful and flexible numerical method that has been widely used in a variety of fields. The Galerkin method is an example of a weighted residual method, where the residual is multiplied by a set of weighting functions and integrated over the domain. The choice of weighting functions is important, and the Galerkin method uses the same basis functions as the approximation functions. The resulting integral equations are then discretized using numerical integration techniques to produce a linear system of equations. After meshing, the software continuously calculates the solution error and when the error value becomes lower than a certain value the software converges. The mesh can also be changed in order to achieve the accurate result.

Since the FEM is used to tackle the issue the first step of solving the problem is to specify the type of meshing. The geometry domain has become into a number of unstructured and adaptive triangular elements. Fig. 2 shows the area's meshing process. As it is known, it is important to check the Sufficiency of the number of Elements in order to reach the high accuracy and low-time processing. Fig. 3
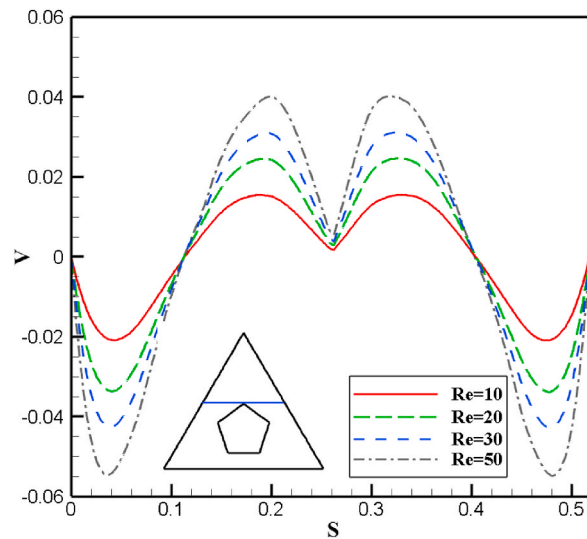
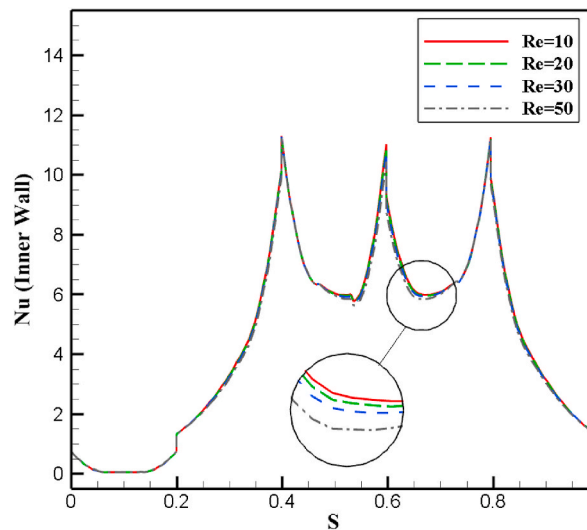**Fig. 12.** Variation of V-velocity respect to different Re

Fig. 13. Variation of *Nu* number respect to different Re

shows the local *Nu* value of inner walls for three different grid sizes of 6988, 19264 and 48632. When $\mathrm{Re} = 20, Ha = 10, Br = 5, Ri = 3, \mathrm{Pr} = 6.2$ and $Le = 1$. According to the reasons stated above if the number of elements is considered 19264, the local Nusselt number will change slightly and will reach almost a reliable value. As a result, grid independency happened and there is no need to increase the number of nodes. To evaluate the efficacy of the suggested method, it is important to compare the results with previous studies. For this purpose, Fig. 4 displays comparison results of temperature profile of enclosure between our numerical method with Khanafer et al. [31]. The geometry used for first validation is a simple two-dimensional rectangular enclosure with heated and cooled walls, filled with a water-based nanofluid and featuring a single spherical nanoparticle that is varied in position to investigate its effect on heat transfer. This figure demonstrates that there is a good agreement between this study's method and their method in order to calculate temperature in the enclosure. Haq et al. [23] conducted research on a trapezoidal cavity with an inner heated obstacle, partially filled with water functionalized with CuO nanoparticles. Fig. 5 compares the results of V-velocity profile between their method with the proposed approach of present study. It is obvious that there is a great agreement between present study and both mentioned researches.

4. Results and discussion

In the following section the effects of changing the values of Ri from 0.01 to 5, Re from 10 to 50, *Ha* from 0 to 20 and Br from 0.01 to 10 on flow field, temperature, concentration, Local Nusselt number in a triangular cavity containing a hexagonal obstacle will be
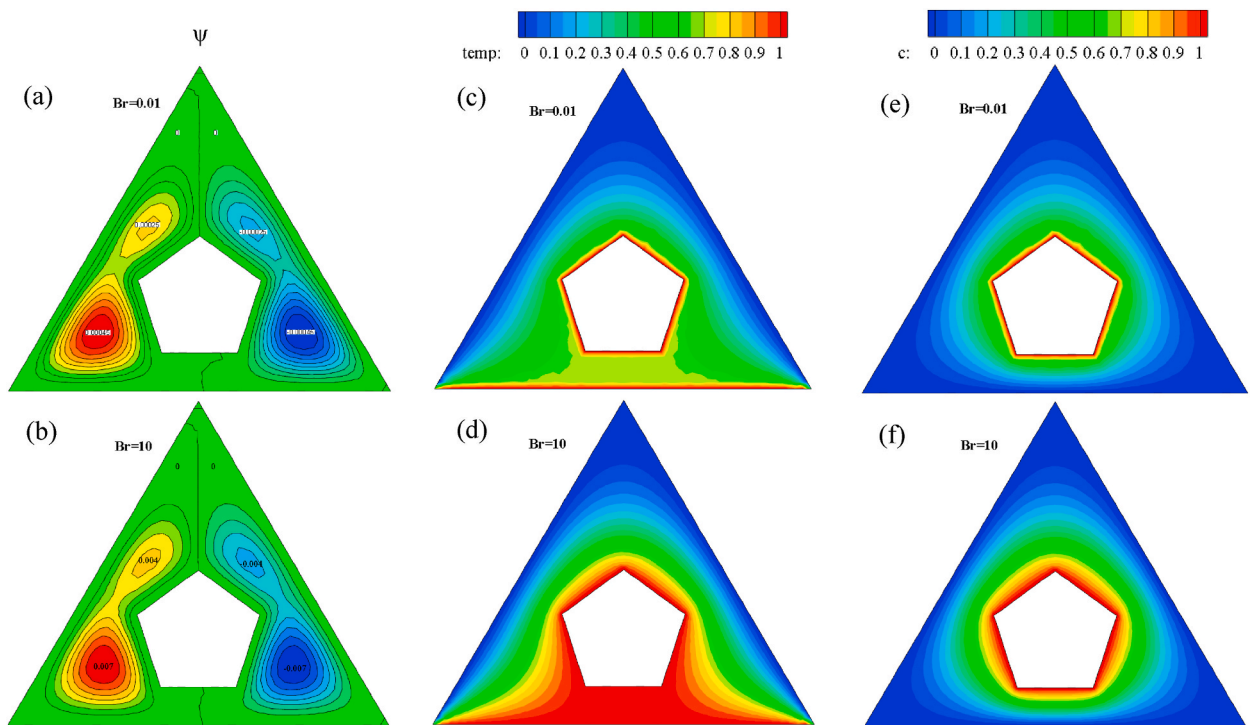
Fig. 14. Variation of (a–b) streamlines, (c–d) isotherms and, (e–f) concentration based on different Br parameters.
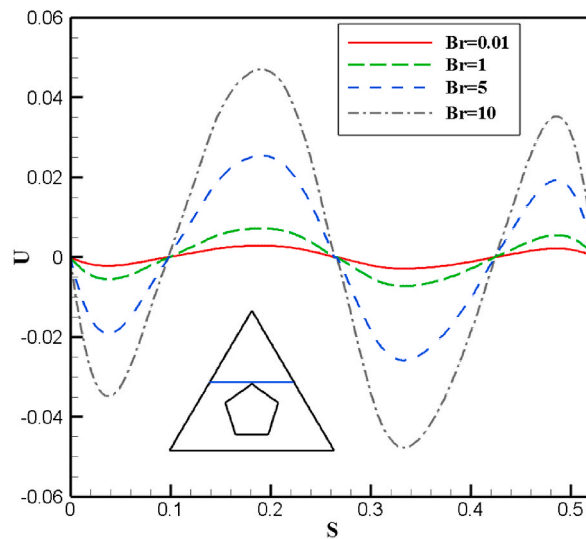

Fig. 15. Variation of U-velocity respect to different Br.

numerically considered and shown.

4.1. Impacts of variations in the Richardson number

Fig. 6 shows the impact of several values of Richardson number on streamlines, isotherms and concentration. Fig. 6(a and b) presents the variation of Ri effects on streamlines. In all Ri values there are some positive and negative recirculation motions in left and right side of the cavity respectively. Meanwhile by increasing the values of Ri from 0.01 to 5 the small effect of forced convection on streamlines changes into larger impact due to increasing the buoyancy term, which means the streamlines are Under the influence of natural and forced convection both. Fig. 6(c and d) displays the consequences of changes of Ri on temperature field. By comparing the
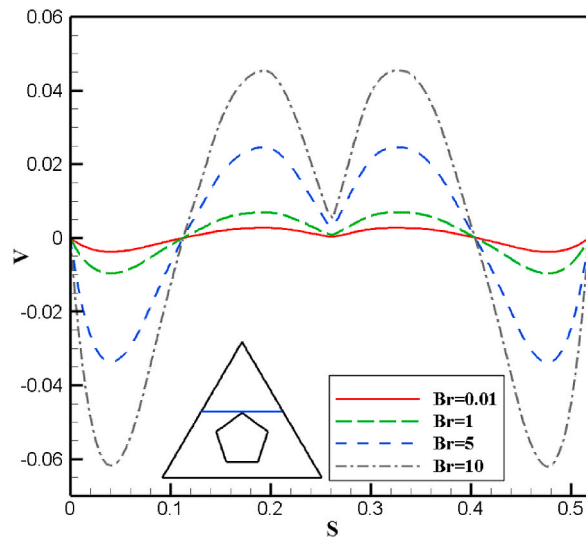
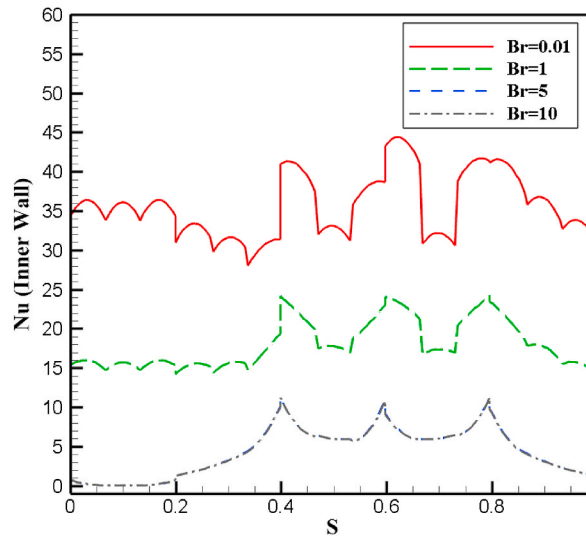**Fig. 16.** Variation of V-velocity respect to different Br.

Fig. 17. Variation of *Nu* number respect to different Br.

thermal contours between Ri = 0.01 and Ri = 5 it could be concluded that the temperature profile decreases. As the result of the growth of the mixed convection movement mechanism due to the Ri increment from Ri = 1 to Ri = 5, the temperature contours also rise. Contours of concentration are given in Fig. 6(e and f) respect to values of Ri. According to the figure the concentration field decreases from Ri = 0.01 to Ri = 5 but for higher values of Ri the concentration value increases again due to the involving of natural convection and as the subsequence, significant mass transfer is happened in the form of heat. Fig. 7 exhibits the effect of variations of Richardson number on U-velocity along the certain line which is shown as a blue line in triangular cavity. The horizontal velocity has fluctuating behavior, meanwhile by increasing the value of Ri this behavior increases dramatically. Fig. 8 depicts the V-velocity changes due to four different values of Ri on mentioned line in cavity picture. The curves show that for all Richardson numbers the vertical velocity in both beginning and end of the line have negative values and similar behavior but in center these curves have positive values. Also all curves have a symmetric shape toward the mentioned line. Fig. 9 describes the variation of *Nu* on pentagonal obstacle based on different Richardson numbers. It is obvious that changing the Ri have no significant impact on Nusselt number for inner wall.

4.2. Impacts of variations in the Reynolds number

The impacts of different values of Re on the streamlines, contour of temperature and concentration can be seen in Fig. 10. The variations of streamlines on four values of Re are shown in Fig. 10(a and b). The results are given for Re = 10 and 50. For Reynolds = 10
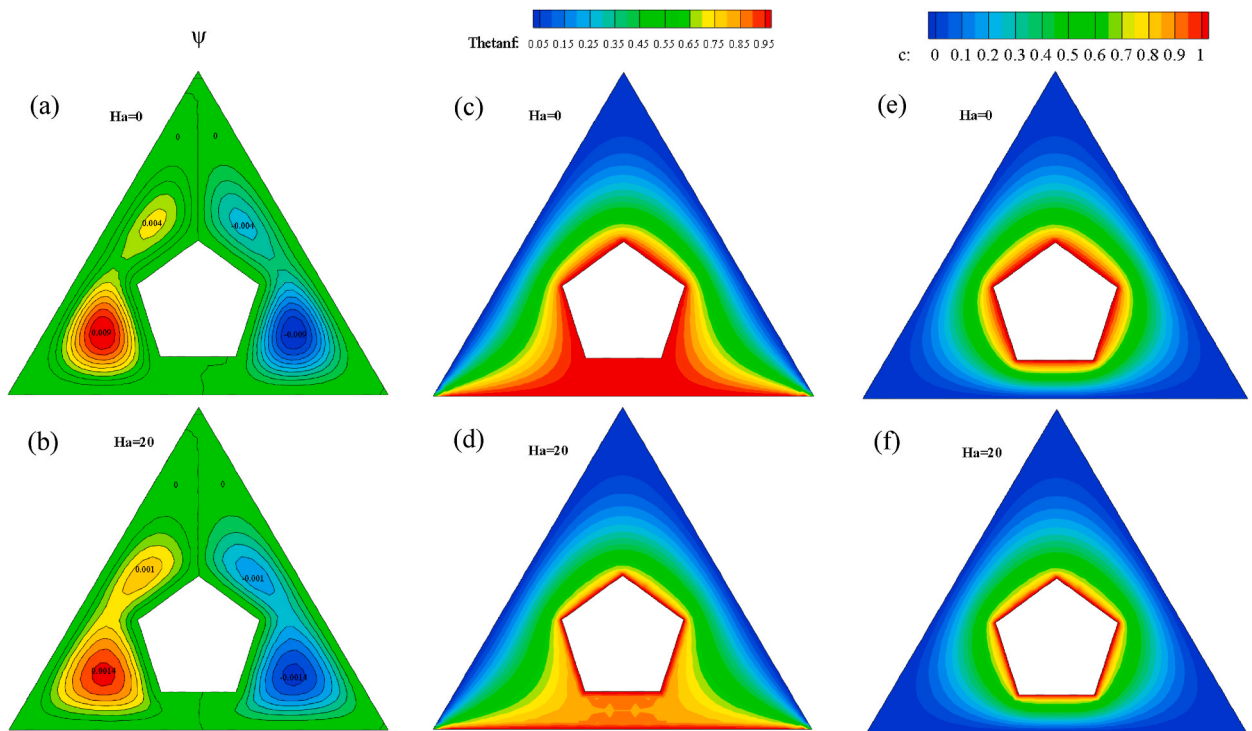
Fig. 18. Variation of (a–b) streamlines, (c–d) isotherms and, (e–f) concentration based on different *Ha* numbers.
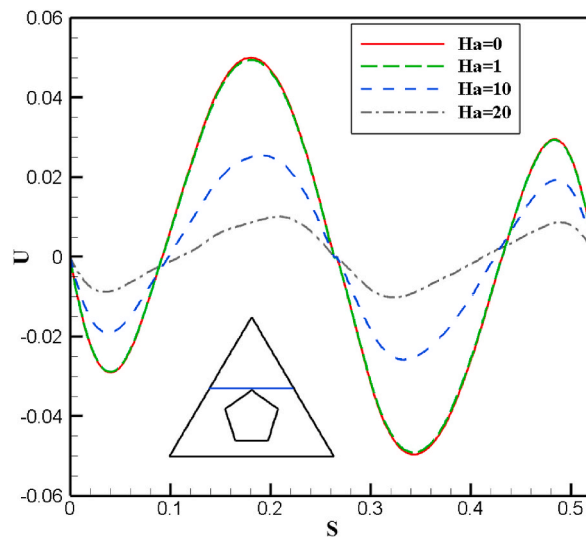

Fig. 19. Variation of U-velocity respect to different *Ha*..

two rotational movements are visible near of two inclined walls of triangle. The left movement has positive and the right one has negative values. With increase of Re from 10 to 50 the magnitude of positive and negative movements increases but the shapes of streamlines are quite stable. Fig. 10(c and d) indicates the influence of variable amount of Re on thermal behavior of cavity in form of isotherms. As expected, there are more heated zones near the lower wall of triangle and pentagonal obstacle's walls. Since the lower wall of triangle has no movement, there are slight changes in isotherm contours by changing the values of Re. Fig. 10(e and f) depicts the variations of concentration profile for different values of Re. As expected, because of the boundary conditions applied to the pentagonal obstacle, the magnitudes of the concentration near the obstacle walls are more than other zones and by increasing the distance from obstacle the concentration profiles get to lower values. It also could be comprehended that by increment of Reynolds number the concentration profile increases slightly. Fig. 11 displays the Consequences of variations of Reynolds number on horizontal
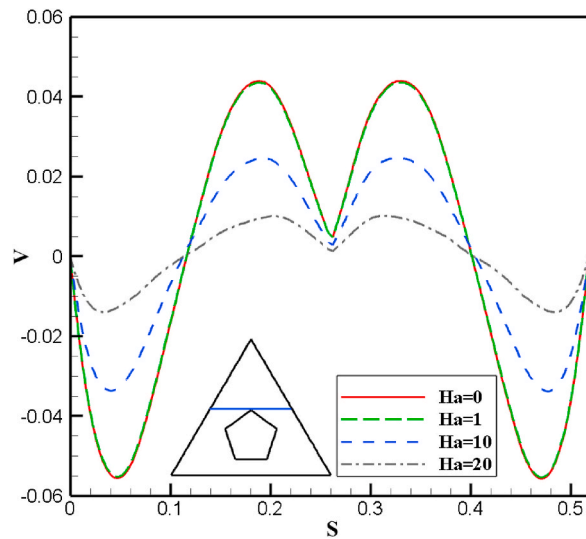
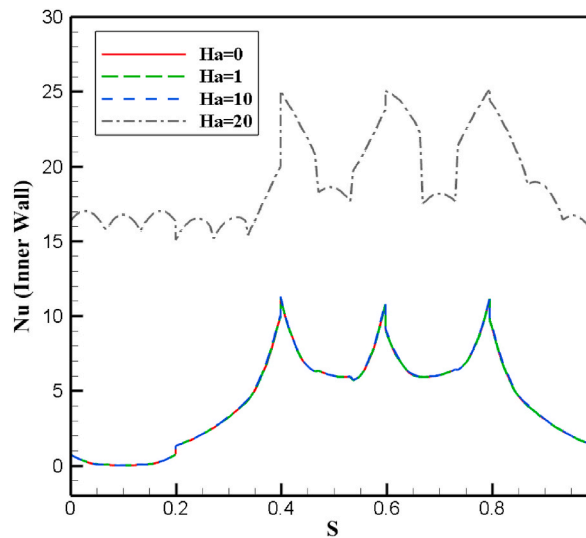**Fig. 20.** Variation of V-velocity respect to different *Ha*..

Fig. 21. Variation of *Nu* number respect to different *Ha*..

velocity along the certain line which is shown as a blue line in triangular cavity. The behavior of the velocity profile in the horizontal direction is similar in certain intervals for diverse values of the Re, meanwhile as the Re has increased, which means the increase of the inertial force, the values of the oscillatory behavior of the U-velocity increase. Fig. 12 demonstrates the V-velocity changes due to four different values of Re on mentioned blue line in cavity. The profiles show that the impacts of various Reynolds number are almost similar to effects of Richardson number on V-velocity diagram. It is clear that higher amounts of Re cause more velocity toward vertical direction. The changes of *Nu* in pentagonal obstacle for various Re are illustrated in Fig. 13. The trend of Nusselt number behavior follows a similar process for all Reynolds number changes. Albeit a slight difference between these values can be seen in the following diagram. Considering the increase of Reynolds number from 10 to 50 along the length of the geometry, the value of Nusselt number at Reynolds 10 is slightly higher than other values. Also, it is obvious that there are three positions with maximum Nusselt number value of almost 11.

4.3. Impacts of variations in the buoyancy ratio parameter

The effects of several Br values on heat transfer, concentration, and streamline in the cavity with a pentagonal obstacle inside have been covered in this section of the article. The definition of Br in this cavity was given in eq. (13) as the ratio of concentration changes to temperature changes impact on buoyancy force. Fig. 14 indicates how three different contours of the cavity are affected by

Table 1
Designed tests by Taguchi approach.

Case Number	Richardson	Reynolds	Brinkman	Hartmann
1	0.01	10	0.01	0
2	5	50	0.01	10
3	5	10	10	1
4	3	50	1	0
5	3	30	0.01	1
6	1	50	5	1
7	0.01	30	5	10
8	3	10	5	20
9	5	20	5	0
10	1	20	0.01	20
11	5	30	1	20
12	3	20	10	10
13	1	10	1	10
14	1	30	10	0
15	0.01	50	10	20
16	0.01	20	1	1

Buoyancy ratio in the range of 0.01–10. Fig. 14(a and b) display recirculation movement in the both sides of the pentagonal barrier with varying symmetry values that change as the Br increases or decreases. In all values of the Br, the recirculation movements have the same overall form in all contours of the streamline, but their values vary at the maximum and minimum areas. Figures (c–d) represent the effects of variation of Br parameter on heat transfer and isotherm contours in wide range of 0.01–10. With an accurate comparison between the figures (c–d), it is clear that increasing the Br parameter has remarkable impacts on rate of heat transfer in cavity. At Br = 0.01 a thin hot layer of fluid is close near to hot walls while increasing Br parameter leads to increment the extent of hot areas between pentagonal obstacle and bottom hot wall. The concentration contours in the various Br are shown in Fig. 14(e and f). Increase of Mass transfer in these contours is obvious due to an increase in buoyancy ratio, which is clearly visible in the contours surrounding the pentagonal barrier. The variation of horizontal velocity changes on the blue line above the obstacle which is shown in mentioned figure due to changes of Br parameter is illustrated in Fig. 15. There is a fluctuating behavior for U-velocity in all Br parameters. In addition, rising the Br parameter led to higher values of U-velocity in a certain position. As the buoyancy ratio (which is the ratio of the density difference to the average density) increases, the buoyancy forces become stronger and the velocity of fluid motion increases. The variation of vertical velocity for different Br parameters was shown in Fig. 16. Regarding mentioned figure the fluid has experienced the peak V-velocity in two symmetric positions. Also, the increase of Buoyancy ratio parameter led to rise of fluctuating behavior of V-velocity. Fig. 17 demonstrates impact of Buoyancy ratio on *Nu* number on inner wall. It can be seen that growth of the Br parameter has reverse impact on *Nu* for inner wall. Also, the fluctuating behavior of the trend of curves for all Buoyancy ratio parameter is visible. Unexpectedly, For Br = 5 and 10 the related curves experienced an overlap.

4.4. Impacts of variations in the Hartmann number

Fig. 18 displays the impacts of *Ha* 0 and 20, which indicates the electromagnetic force influence in the studied cavity. Hartmann equals to zero is considered as there is no electromagnetic force. Fig. 18(a and b) shows the effect of the *Ha* which gradually increases on the streamline in the cavity. At *Ha* = 0, the top values appear symmetrically opposite of each other with contrariwise circulation movements. On the left wall of the pentagonal obstacle, the maximum value of the flow function (0.09) and the minimum value at the bottom right side (−0.09) is displayed. With an increase in the *Ha*, the shape of the streamline remains constant, but their values have changed. Fig. 18(c and d) show how the temperature contours for different Hartmann numbers in which around the pentagonal obstacle and the lower wall of the cavity, the maximum temperature is visible. As the raise in the electromagnetic force's intensity, the maximum temperature range begins to narrow as it gets closer to the bottom triangular wall and the obstacle. With an increase in the *Ha* from 0 to 20, we observe a decrease in the maximum concentration around the pentagonal barrier in Fig. 18(e−f). According to the results of variations in the electromagnetic force's intensity within this cavity caused by the used boundary conditions, the overall magnitude of the concentration has been decreased. Fig. 19 demonstrates the trend of changing U-velocity based on different values of Hartmann number which shows how electromagnetic force effects on the mentioned parameter. From Fig. 19 it is clear that increasing the *Ha*, the lowest and the highest U-velocity in a certain point has been decreased. Fig. 20 illustrates the symmetrical behavior of the vertical velocity relative to the given blue line's middle point, similar to the other vertical velocity graphs presented in the preceding sections. As the electromagnetic force gets stronger, electric vortexes are created inside the fluid flow, which create restance to the movement of the fluid flow and reduce the horizontal and vertical velocities both. Fig. 21 expresses the effect of *Ha* on Nusselt number for pentagonal obstacle walls, in which the difference between *Ha* = 0, 1 and 10 is negligible and is almost unchanged, whereas a sudden jump in results for *Ha* = 20 is observed, which shows that the impressive effect of electromagnetic force is happening on *Nu*.

4.5. Optimizing parameters and correlation derive

The main purpose of this section is to reach optimum values for four main parameters which are studied above. Each of the four
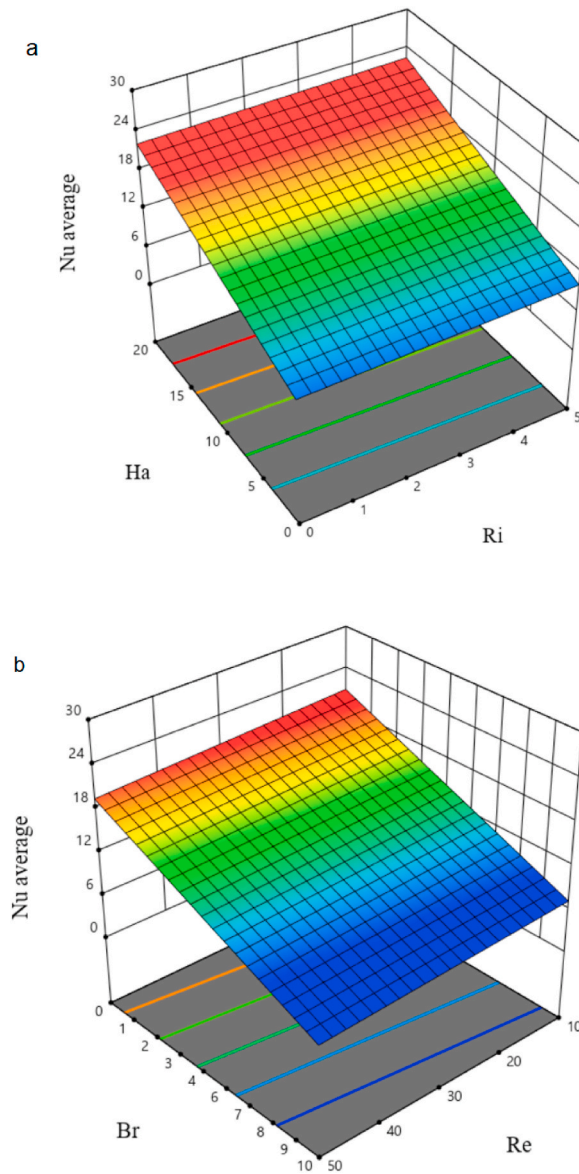
Fig. 22. Effects of (a) Ri and *Ha* (b) Br and Re on average *Nu* number by RSM.

mentioned parameters changes four time. Hence, in order to get the optimum value, 4^4 different modes should be examined totally. But with the help of Taguchi's method, the number of tests is reduced to 16, which leads to reduction of the processing time, increase of the accuracy and achieving a reliable answer. The 16 different cases determined by Taguchi's method are detailed in Table 1.

With the help of the Design- Expert software the RSM (Response surface method) is used to design an experiment considering these 16 different cases. The goal in the response surface method is to optimize the response that is affected by several independent input variables, which in this study the response is the Average eNu. A second-order pseudo-polynomial model is used in place of the first-order model once the RSM achieves the optimal point. To estimate the optimal position, a quadratic polynomial pseudo model is employed. The estimated optimal point is tested to determine whether it is actually optimal in the final stage. Equation (20) exhibits a sample second-order pseudo-polynomial. In the given formula, *y* is assumed as Nu_{avg}, x_i and x_j are independent input variables and constant coefficients are displayed as a_i and the error value is specified as ξ.

$$y = a_0 + \sum_{i=1}^{n} a_i x_i + \sum_{i=1}^{n} a_{ii} x_i^2 + \sum_{i=1}^{n} \sum_{j=1}^{n} a_{ij} x_i x_j \big|_{i<j} + \xi \tag{20}$$

Fig. 22 (a) demonstrates three-dimensional RSM analysis of average Nusselt number changes versus various Hartmann and Ri. It's shown that the increment of Ri has a negligible effect on average *Nu* changes, but on the contrary. As Ri raises, the value of the *Nu* also
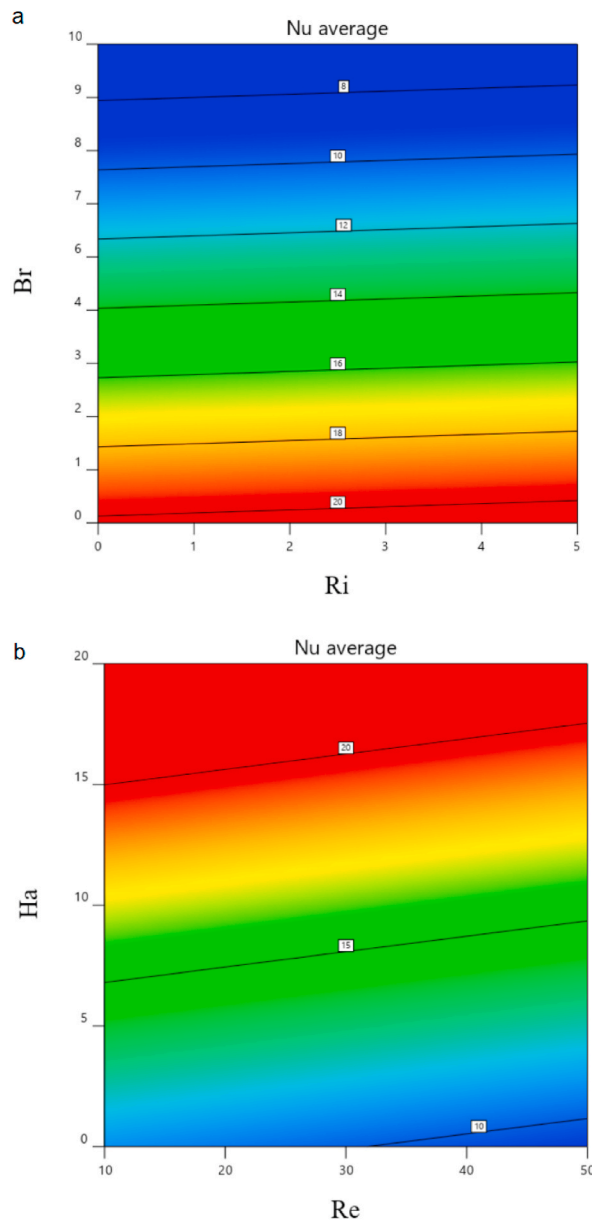
Fig. 23. Effects of (a) Ri and Br (b) *Ha* and Re on average *Nu* number by RSM.

Table 2
The Analysis of Variance table (ANOVA).

Source	Sum of Squares	df	Mean Square	F-value	p-value	
Model	868.68	4	217.17	14.84	0.0002	significant
A-Ri	0.4823	1	0.4823	0.0330	0.8592	
B–Re	5.32	1	5.32	0.3633	0.5589	
C–Br	474.05	1	474.05	32.40	0.0001	
D-Ha	388.83	1	388.83	26.57	0.0003	
$R^2 = 0.874$						

increases dramatically. How the average Nusselt number reacts in response to variations in Br and Re is depicted in a three-dimensional plot in Fig. 22(b). According to the mentioned figure, the Nusselt number's slope of variation with a change in Reynolds number is noticeably lower than the slope of changes in Nusselt number with a change in Buoyancy ratio parameter. Fig. 23 (a, b) illustrates 2-D
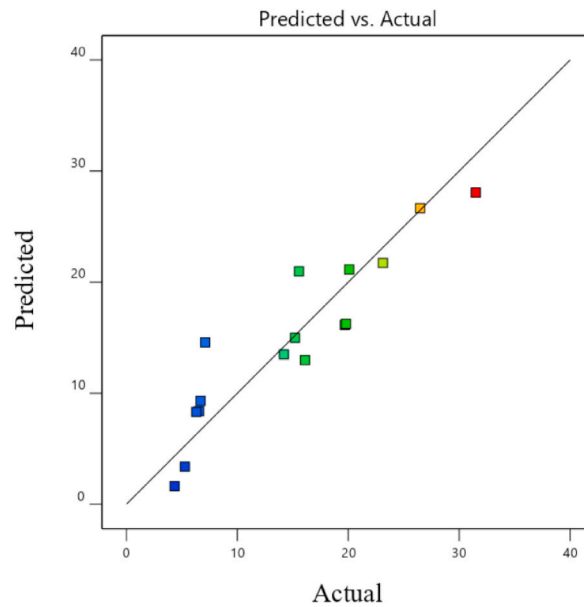
Fig. 24. Comparison between predicted and actual average Nusselt number.

Table 3
Optimum values of the parameters by RSM.

Parameter	Optimum value
Ri	4.95
Re	30.49
Br	0.05
Ha	18.35

analysis of optimal values of two studied parameters versus average *Nu* which is the result of RSM. Equation (21) unveils a correlation in order to determine Nu_{avg} as a function of four dimensionless major studied parameters.

$$Nu_{average} = 16.548 - 0.0905(Ri) - 0.0389(\text{Re}) - 1.383(Br) + 0.6105(Ha) \qquad (21)$$

After predicting this mathematical correlation, the regression model's overall validity is examined using the data's analysis of variance (ANOVA). Table 2 displays the ANOVA for the mentioned equation (21). The coefficient of determination (R^2) of the models shows the probability that the proposed software model is correct. With the analysis, the coefficient is 87.4% which shows the agreement of the suggested method with real output data.

Fig. 24 shows the anticipated versus real values of Nu_{avg} for sixteen different cases of optimization experiment. It appears that there is strong agreement between the predicted and the actual results. Hence, the RSM correlation is appropriate and reliable. After utilization of the RSM and ANOVA table, output data of the optimum value of four major examined parameters are listed in Table 3. Hence, by substituting this optimum data into the suggested average Nusselt number correlation in Eq (21), leads to achieve maximum amount of average *Nu* for the studied cavity.

5. Conclusion

MHD mixed convection in a triangular cavity with a pentagonal obstacle was investigated for several effective parameters such as Ri, Re, *Ha* and Br on flow field, isotherm, concentration, velocity and Nusselt number. For each of the aforementioned parameters four different values were considered. Also, the optimization of the investigated dimensionless parameters was also accomplished with the aid of the Taguchi approach and RSM, and a correlation for getting the optimum average *Nu* in the specified cavity was ultimately derived. The study's results are summarized in the section below:

- Increasing the Re causes low decrement in *Nu* and heat transfer.
- Buoyancy ratio changes have reverse behavior with Nusselt number and with increment in Br parameter, the temperature profile in cavity around the pentagonal obstacle rises dramatically.
- A correlation was derived with the help of the Taguchi and RSM method for achieving the optimum value for *Nu* in order to maximize the heat transmission.

Author contribution statement

Kh. Hosseinzadeh: Conceived and designed the analysis; Analyzed and interpreted the data; Contributed analysis tools or data.
M. Roshani, M.A. Attar: Contributed analysis tools or data; Wrote the paper.
D.D. Ganji, Mohammad Behshad Shafii: Contributed analysis tools or data.

Data availability statement

Data will be made available on request.

Declaration of competing interest

The authors declare that they have no known competing financial interests or personal relationships that could have appeared to influence the work reported in this paper.

Acknowledgment

References

[1] Han-Taw Chen, Yao-Lun Chang, Pei-Yu Lin, Yu-Jie Chiu, Jiang-Ren Chang, Numerical study of mixed convection heat transfer for vertical annular finned tube heat exchanger with experimental data and different tube diameters, Int. J. Heat Mass Tran. 118 (2018) 931–947.
[2] V.K. Mathew, Hotta Tapano Kumar, Numerical investigation on optimal arrangement of IC chips mounted on a SMPS board cooled under mixed convection, Therm. Sci. Eng. Prog. 7 (2018) 221–229.
[3] Etienne Wurtz, Jean-Michel Nataf, Frederick Winkelmann, Two-and three-dimensional natural and mixed convection simulation using modular zonal models in buildings, Int. J. Heat Mass Tran. 42 (5) (1999) 923–940.
[4] Chao Xiao, Qiang Liao, Qian Fu, Yun Huang, Ao Xia, Hao Chen, Xun Zhu, Numerical investigation of laminar mixed convection of microalgae slurry flowing in a solar collector, Appl. Therm. Eng. 175 (2020) 115366.
[5] Mohammad Reza Tavakoli, Omid Ali Akbari, Anoushiravan Mohammadian, Erfan Khodabandeh, Farzad Pourfattah, Numerical study of mixed convection heat transfer inside a vertical microchannel with two-phase approach, J. Therm. Anal. Calorim. 135 (2) (2019) 1119–1134.
[6] Adnan M. Hussein, R.A. Bakar, K. Kadirgama, Study of forced convection nanofluid heat transfer in the automotive cooling system, Case Stud. Therm. Eng. 2 (2014) 50–61.
[7] Mohsen Sheikholeslami, Mofid Gorji-Bandpy, Kuppalapalle Vajravelu, Lattice Boltzmann simulation of magnetohydrodynamic natural convection heat transfer of Al2O3–water nanofluid in a horizontal cylindrical enclosure with an inner triangular cylinder, Int. J. Heat Mass Tran. 80 (2015) 16–25.
[8] Wael Al-Kouz, Aiman Alshare, Suhil Kiwan, Ahmad Al-Muhtady, Alkhalidi Ammar, Haneen Saadeh, Two-dimensional analysis of low-pressure flows in an inclined square cavity with two fins attached to the hot wall, Int. J. Therm. Sci. 126 (2018) 181–193.
[9] Rizwan Ul Haq, Feroz Ahmed Soomro, Hakan F. Öztop, Toufik Mekkaoui, Thermal management of water-based carbon nanotubes enclosed in a partially heated triangular cavity with heated cylindrical obstacle, Int. J. Heat Mass Tran. 131 (2019) 724–736.
[10] Waqar A. Khan, Zafar H. Khan, Mixed convection of single-walled carbon nanotubes in a triangular cavity containing a pentagonal impediment, in: IOP Conference Series: Materials Science and Engineering, vol. 839, IOP Publishing, 2020, 012021, 1.
[11] Abdalla M. Al-Amiri, Khalil M. Khanafer, Ioan Pop, Numerical simulation of combined thermal and mass transport in a square lid-driven cavity, Int. J. Therm. Sci. 46 (7) (2007) 662–671.
[12] Apurba Kumar Santra, Swarnendu Sen, Niladri Chakraborty, Study of heat transfer augmentation in a differentially heated square cavity using copper–water nanofluid, Int. J. Therm. Sci. 47 (9) (2008) 1113–1122.
[13] B. Ghasemi, S.M. Aminossadati, Mixed convection in a lid-driven triangular enclosure filled with nanofluids, Int. Commun. Heat Mass Tran. 37 (8) (2010) 1142–1148.
[14] S. Sivasankaran, V. Sivakumar, P. Prakash, Numerical study on mixed convection in a lid-driven cavity with non-uniform heating on both sidewalls, Int. J. Heat Mass Tran. 53 (19–20) (2010) 4304–4315.
[15] M. Hasanuzzaman, M.M. Rahman, Hakan F. Öztop, N.A. Rahim, R. Saidur, Effects of Lewis number on heat and mass transfer in a triangular cavity, Int. Commun. Heat Mass Tran. 39 (8) (2012) 1213–1219.
[16] Litan Kumar Saha, Km Salah Uddin, M.A. Taher, Effect of internal heat generation or absorption on MHD mixed convection flow in a lid driven cavity, Am. J. Appl. Math. 3 (1–1) (2015) 20–29.
[17] Faroogh Garoosi, Behzad Rohani, Mohammad Mehdi Rashidi, Two-phase mixture modeling of mixed convection of nanofluids in a square cavity with internal and external heating, Powder Technol. 275 (2015) 304–321.
[18] Rizwan Ul Haq, S. Naveed Kazmi, Toufik Mekkaoui, Thermal management of water based SWCNTs enclosed in a partially heated trapezoidal cavity via FEM, Int. J. Heat Mass Tran. 112 (2017) 972–982.
[19] Soomro, Ahmed Feroz, Z. Hammouch, Heat transfer analysis of CuO-water enclosed in a partially heated rhombus with heated square obstacle, Int. J. Heat Mass Tran. 118 (2018) 773–784.
[20] Wael Al-Kouz, Aiman Alshare, Suhil Kiwan, Ahmad Al-Muhtady, Alkhalidi Ammar, Haneen Saadeh, Two-dimensional analysis of low-pressure flows in an inclined square cavity with two fins attached to the hot wall, Int. J. Therm. Sci. 126 (2018) 181–193.
[21] M. Munshi, Jahirul Haque, Golam Mostafa, A.B.S. Manik Munsi, Md Waliullah, Hydrodynamic mixed convection in a lid-driven hexagonal cavity with corner heater, Am. J. Comput. Math. 8 (3) (2018) 245.
[22] Fatih Selimefendigil, Mixed convection in a lid-driven cavity filled with single and multiple-walled carbon nanotubes nanofluid having an inner elliptic obstacle, Propulsion and power research 8 (2) (2019) 128–137.
[23] Rizwan Haq, Sidra Aman, Water functionalized CuO nanoparticles filled in a partially heated trapezoidal cavity with inner heated obstacle: FEM approach, Int. J. Heat Mass Tran. 128 (2019) 401–417.
[24] Shantanu Dutta, Navneet Goswami, Arup Kumar Biswas, Sukumar Pati, Numerical investigation of magnetohydrodynamic natural convection heat transfer and entropy generation in a rhombic enclosure filled with Cu-water nanofluid, Int. J. Heat Mass Tran. 136 (2019) 777–798.

[25] Rizwan Ul Haq, Shah Syed Saqib, Ebrahem A. Algehyne, Iskander Tlili, Heat transfer analysis of water based SWCNTs through parallel fins enclosed by square cavity, Int. Commun. Heat Mass Tran. 119 (2020), 104797.

[26] S. Saqib Shah, Rizwan Ul Haq, Wael Al-Kouz, Mixed convection analysis in a split lid-driven trapezoidal cavity having elliptic shaped obstacle, Int. Commun. Heat Mass Tran. 126 (2021), 105448.

[27] M. Bahiraei, N. Mazaheri, M.R. Daneshyar, A. Mwesigye, Two-phase simulation of irreversibilities for Ag–water nanofluid flow inside an elliptical pin-fin heat sink: entropy generation and exergy considerations, Powder Technol. 409 (2022), 117723.

[28] M. Bahiraei, A numerical study of heat transfer characteristics of CuO–water nanofluid by Euler–Lagrange approach, J. Therm. Anal. Calorim. 123 (2016) 1591–1599.

[29] M. Amani, P. Amani, M. Bahiraei, M. Ghalambaz, G. Ahmadi, L.P. Wang, O. Mahian, Latest developments in nanofluid flow and heat transfer between parallel surfaces: a critical review, Adv. Colloid Interface Sci. 294 (2021), 102450.

[30] N. Mazaheri, M. Bahiraei, Energy, exergy, and hydrodynamic performance of a spiral heat exchanger: process intensification by a nanofluid containing different particle shapes, Chemical Engineering and Processing-Process Intensification 166 (2021), 108481.

[31] K. Khanafer, K. Vafai, M. Lightstone, Buoyancy-driven heat transfer enhancement in a two-dimensional enclosure utilizing nanofluids, Int. J. Heat Mass Tran. 46 (19) (2003) 3639–3653. .

Nomenclature

Roman letters

B: electromagnetic force intensity
Br: buoyancy ratio
c: species concentration
C: dimensionless species concentration
D: mass diffusivity (m3/s)
g: gravitational acceleration (m/s2)
Ha: Hartmann number
L: characteristic length scale
Le: Lewis number
Nu: Local Nusselt number
p: Pressure
P: dimensionless pressure
Pr: Prandtl number
Re: Reynolds number
Ri: Richardson number
T: temperature (K)
(u, v): velocities component in the x- and y-directions $\left(m/_s\right)$
(U, V): Dimensionless velocities component in the x- and y-directions
(x, y): coordinates (m)
(X, Y): dimensionless coordinates
(x_i, x_j): RSM independent input variables

Greek symbols

α: thermal diffusivity (m2/s)
β_c: coefficient of solutal expansion (m3/kg)
β_T: coefficient of thermal expansion (K-1) (m2/s)
γ: Penalty parameter
θ: dimensionless temperature
μ: dynamic viscosity of the fluid $\left(kg/_{m.s}\right)$
υ: kinematic viscosity of the fluid $\left(m^2/_s\right)$
ρ: density of the fluid $\left(kg/_{m^3}\right)$
ζ: RSM polynomial error value
σ: electrical conductivity $\left(S/_m\right)$
ψ: dimensionless stream function

Subscripts

0*:* reference state
avg: Average
c: Cold wall
h: Hot wall